ChemComm

COMMUNICATION

View Article Online
View Journal | View Issue

Cite this: *Chem. Commun.*, 2026, **62**, 965

Received 29th October 2025,
Accepted 4th December 2025

DOI: 10.1039/d5cc06149k

rsc.li/chemcomm

Lateral size modulated structural color of aqueous dispersions of titanate nanosheets

Takayuki Kikuchi, [ab] Yasuo Ebina, [a] Nobuyuki Sakai, [a] Yoshiyuki Sugahara, [bc] Takayoshi Sasaki *[a] and Renzhi Ma *[ab]

Deionized suspensions of titanate nanosheets exhibit vivid structural colors arising from the formation of lamellar liquid-crystalline phases. We investigated the impact of lateral size on the resulting structural coloration. A decrease in average lateral size (aspect ratio) shifts the structural color toward a blue dominant tone and narrows the reflection bandwidth, indicating an improvement in structural regularity. This behavior can be attributed to the faster orientational relaxation of smaller nanosheets, which may promote better alignment to enhance color purity. The current study establishes lateral-size modulation as a practical and broadly applicable strategy for achieving higher color purity in colloidal structural color systems.

Two-dimensional (2D) nanosheets, characterized by their high aspect ratio (lateral size *vs.* thickness), are known to form liquid-crystalline lamellar phases in dispersion.[1] Extensive reduction in the ionic strength of nanosheet dispersions greatly expands the lamellar (intersheet) spacing, thereby inducing structural coloration *via* optical interference in the visible range.[2] Structural colors arising from such self-assembled lamellar architectures are promising for applications including sensing[3] and security printing,[4] wherein a narrow reflection bandwidth (*i.e.*, high color purity) is essential. Several reports have noted effects of lateral size on structural color purity in 2D colloids.[5–7] A recent study on photonic crystals of graphene oxide (GO) demonstrated size-dependent optical responses under magnetic-field alignment.[6] However, GO shows optical absorption in the visible light range, which complicates the isolation of pure structural-color metrics, such as the peak reflectance and full width at half maximum (FWHM), from absorptive contributions attributable to the π–π* and *n*–π* electronic transitions.[8] In this aspect, metal oxide nanosheets, which generally do not absorb visible light and possess a high refractive index,[9] are suitable for systematic studies on lateral size modulated structural color. Among them, $Ti_{0.87}O_2$ nanosheets stand out due to their multifunctionality such as a high photocatalytic activity,[10] magnetic and magneto-optical responsivity upon doping with transition-metals (*e.g.*, Fe, Co),[11] *etc.*

In the current study, we explore size-modulated structural coloration of aqueous suspensions of $Ti_{0.87}O_2$ nanosheets. $Ti_{0.87}O_2$ nanosheets were prepared following an established protocol reported in the literature.[2b,12] Polycrystalline $K_{0.8}Ti_{1.73}Li_{0.27}O_4$ was converted into an acid-exchanged form, which was reacted with tetramethylammonium (TMA) hydroxide (TMA^+/H^+ = 1) to produce gigantically swollen crystals. The swollen sample was subsequently exfoliated into unilamellar nanosheets by mechanical shaking. The obtained suspensions were subjected to sonication for 0, 2, 4, and 8 h to progressively reduce the lateral size. The resulting samples are referred to as T0, T2, T4, and T8, respectively. The absence of any crystal phase transformation of the nanosheets after sonication was confirmed by XRD analysis (Fig. S1).

Deionization cycles were then carried out by repeated sedimentation of the colloidal nanosheets by centrifugation (29 300 g, 1 h) and their redispersion with ultrapure water (> 10 cycles), yielding ionic conductivities ≤ 0.01 mS cm^{-1}, at which the $Ti_{0.87}O_2$ nanosheets exhibited a ζ potential below −70 mV in water. The deionized suspension was then injected into a home-made cell with a thin gap of 0.13 mm to observe the structural color.[2b] Diffuse reflectance spectra including the specular component were measured at normal incidence using an integrating sphere with a standard white reference.

Fig. 1 shows atomic force microscopy (AFM) images of $Ti_{0.87}O_2$ nanosheets after sonication for different duration. All samples showed an apparent monolayer thickness of 1.1 nm (Fig. S2), and mean lateral size decreased monotonically with extended sonication time. Fig. S3 shows lateral-size distributions fitted with a log-normal function. The mean lateral size decreases from 3.9 μm to 1.4, 0.73, and 0.37 μm after sonication for 2, 4, and 8 h, respectively. As shown in Table S1, the polydispersity on the logarithmic scale was calculated to be 7.3%, 8.2%, 8.3%, and

[a] *Research Center for Materials Nanoarchitectonics (MANA), National Institute for Materials Science (NIMS), 1-1 Namiki, Tsukuba, Ibaraki 305-0044, Japan. E-mail: SASAKI.Takayoshi@nims.go.jp, MA.Renzhi@nims.go.jp*
[b] *Graduate School of Advanced Science and Engineering, Waseda University, 3-4-1 Okubo, Shinjuku-ku, Tokyo 169-8555, Japan*
[c] *Kagami Memorial Research Institute for Materials Science and Technology, Waseda University, 2-8-26 Nishi-waseda, Shinjuku-ku, Tokyo 169-0051, Japan*

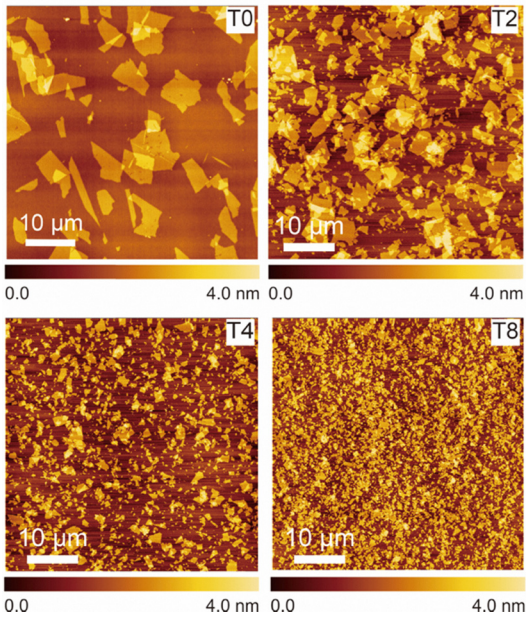

Fig. 1 AFM images of $Ti_{0.87}O_2$ nanosheets sonicated for 0, 2, 4, and 8 h (T0, T2, T4, and T8, respectively).

10.9%, respectively, which are comparable to those previously reported for sonicated niobate nanosheets.[7] Accordingly, all the samples can be considered to exhibit similar polydispersity.

After injecting the deionized suspension into a thin cell, the nanosheets tended to align parallel to the cell face under the shear force. The co-facial orientation of nanosheets helped to form lamellar domains, yielding a vivid structural color (Fig. S4). As shown by the reflectance spectra in Fig. 2, both the peak wavelength λ_{peak} and reflectance intensity were dependent on the concentration of nanosheets. In general, λ_{peak} shifted monotonically to longer wavelengths with decreasing volume fraction φ. In addition, the long-wavelength cutoff decreased from approximately 1150 nm for pristine nanosheets (T0) to about 500 nm for the sonicated sample (T8). Using Bragg's equation $m\lambda = 2n_{av}d \sin\theta$, where m indicates diffraction order and n_{av} represents the averaged refractive index (1.33) of the suspension,[2] the lamellar spacing could be calculated from λ_{peak}. As plotted in Fig. 3, reducing the lateral size generally yielded a decreased intersheet spacing at a fixed volume fraction. A maximum d value of 430 nm was observed for T0 sample without sonication, in contrast with 400, 300, and 188 nm for the sonicated samples T2, T4, and T8, respectively. Consequently, the intersheet spacing and corresponding peak wavelength can be tuned continuously by both concentration and lateral size of nanosheets. Assuming an average lateral size $\langle L \rangle$ of nanosheets with a uniform monolayer thickness t, number density n can be expressed as $n \sim \varphi/t \langle L^2 \rangle$. At a fixed φ, decreasing $\langle L \rangle$ causes an increase in the number density of nanosheets and corresponding osmotic pressure they exert.[13] This enhanced osmotic pressure likely acts as an effective compressive force, leading to a reduction in the intersheet spacing d.

As an indicator of color purity, the reflectance peak near 420 nm for all samples with different sizes were compared in

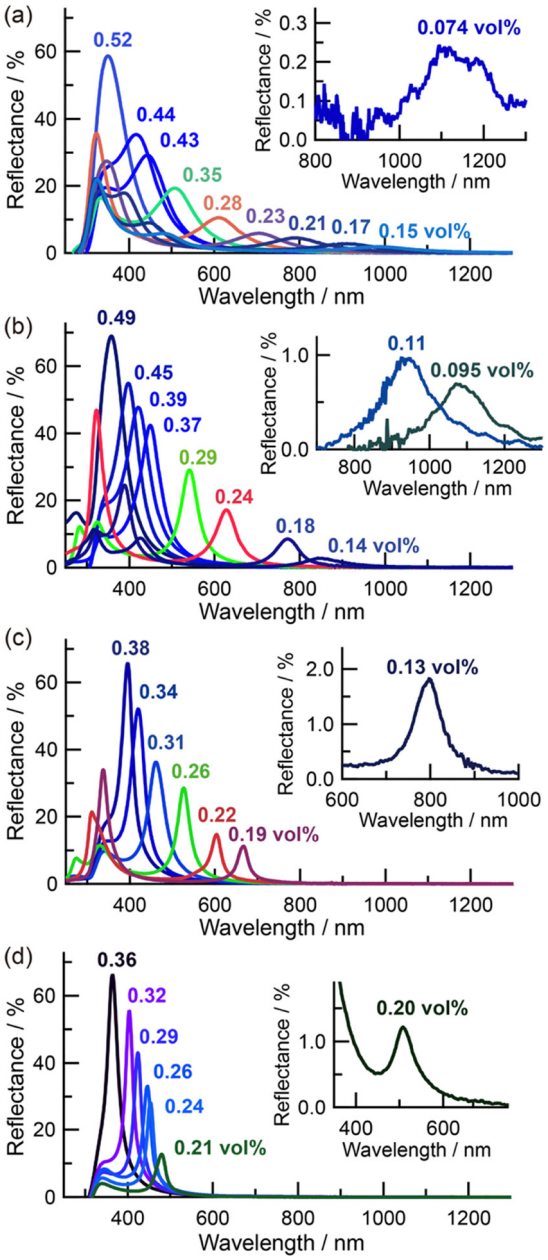

Fig. 2 Reflectance spectra with different volume fractions (vol%) of nanosheets: (a) T0, (b) T2, (c) T4, (d) T8.

Fig. 4. The pristine sample exhibited a very broad band, which became progressively sharpened with reducing the lateral size. Specifically, Lorentzian fits of the reflection peaks yielded an initial FWHM value exceeding 100 nm (T0), which eventually narrowed to less than 25 nm (T8). To further decouple size-dependent effects, FWHM values were plotted across the entire band (Fig. 5). A continuous narrowing trend in the bandwidth was observed with decreasing lateral sizes. In addition, for each series of the same lateral size, lowering the volume fraction produced a red shift of λ_{peak} and a pronounced increase in FWHM, which was accompanied by a decrease in peak reflectance (Fig. S5). Caution is required when interpreting the broadening or narrowing of the FWHM at different

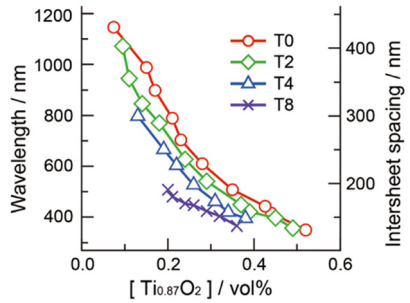

Fig. 3 Peak wavelength and intersheet spacing *versus* volume fraction of nanosheets with different lateral sizes.

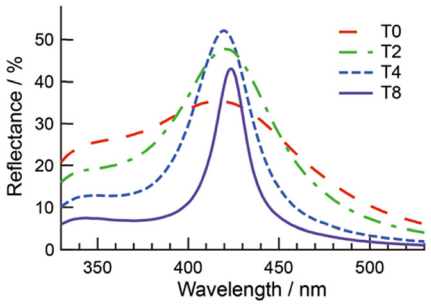

Fig. 4 Comparison of reflectance peaks near 420 nm for nanosheets with different sizes.

wavelengths. By analogy with previous studies on colloidal photonic materials,[14] a dimensionless relative bandwidth, $\Delta\lambda/\lambda_0$—where $\Delta\lambda$ is the FWHM of the reflection peak and λ_0 is the peak maximum—is plotted in Fig. S6. Because photon energy decreases at longer wavelengths and increases at shorter wavelengths, an identical intrinsic photonic bandwidth appears as a larger or smaller FWHM when expressed on the wavelength scale. It is also noteworthy that the peak reflectance was influenced by both the mean lateral size and volume fraction. As shown in Fig. 4, the peak reflectance at 420 nm tended to increase with decreasing mean lateral size. However, this trend became less obvious or even reversed, particularly for smaller-sized nanosheets at low volume fractions (Fig. S5).

Structural color of 2D nanosheets is strongly governed by the underlying liquid-crystalline order. In general, lyotropic

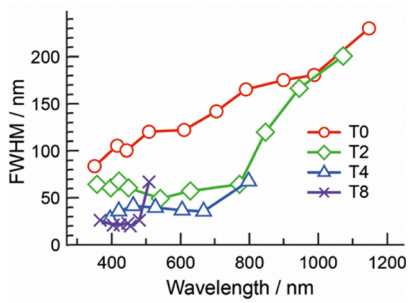

Fig. 5 FWHM plotted as a function of wavelength for nanosheets with different sizes.

liquid-crystalline ordering of high-aspect-ratio colloids emerges once the volume fraction exceeds a critical threshold: the loss of orientational entropy is offset by a gain in translational entropy due to reduced excluded volume, producing an entropy-driven free-energy decrease.[1,7] Under the conditions of high concentration range and low ionic strength where structural color arises, the liquid-crystal phase is formed with different degree of orientational and/or positional ordering:[15] (i) a nematic phase with purely orientational order; (ii) a special columnar nematic phase that exhibits layering periodicity along the layer-normal direction but weak in-plane positional correlations; and (iii) a lamellar phase that combines orientational order with pronounced one-dimensional periodicity and improved in-plane registry (positional correlation). In the current study, structural coloration of $Ti_{0.87}O_2$ nanosheets was derived from the formation of a predominant lamellar phase, *i.e.*, the one-dimensional periodicity.[2] The evolution in peak reflectance and FWHM may be associated with in-plane positional correlations.[6] To verify this, liquid-crystalline textures of deionized $Ti_{0.87}O_2$ nanosheet suspensions were further assessed by polarized optical microscopy (POM). As shown in Fig. 6, the pristine T0 sample exhibited a nematic Schlieren texture with strong interference colors and banded layering feature.[16] The Schlieren texture changed little upon rotation (Fig. S7), indicating non-uniform lamellar alignment and a broad azimuthal distribution of domain orientations. By contrast, these features were absent in the sonicated T4 sample. Instead, vivid blue and yellow regions appeared near the wall surface, which reversed to yellow (−45°) and blue (+ 45°), respectively, upon rotation (Fig. S8), consistent with the formation of left- and right-tilted lamellar domains as previously reported for flow-induced

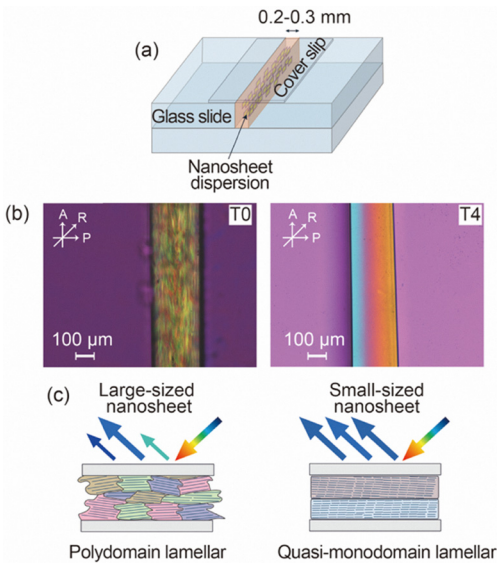

Fig. 6 (a) Schematic illustration of the cell configuration for POM observation; the sample was observed along the cell normal. (b) POM images of pristine T0 and sonicated T4 samples (0.3 vol%). The white arrows labeled A, P, and R indicate the directions of the analyzer, polarizer, and first-order retardation plate (λ: 530 nm), respectively. (c) Schematic representation of possible lamellar domain textures formed by the alignment of nanosheets within the cell.

orientation of nanosheets.[17] Here, a weak shear generated during the cell filling likely served as the aligning field.[7]

Based on the POM assessment, possible lamellar domain textures formed for different-sized nanosheets within the cell are illustrated in Fig. 6c. For large-sized nanosheets, polydomain lamella with differing azimuthal orientations and slight variations in intersheet spacing coexist. As a result, incident white light is reflected over a relatively broad spectral band. For small-sized nanosheets, the texture indicates a quasi-monodomain lamella with a narrowly distributed director and spacing, yielding a small bandwidth, which agrees well with the observed evolving trend. A plausible explanation for this difference is that smaller nanosheets possess greater rotational freedom and can relax more readily towards a common director under transient shear, whereas larger nanosheets experience greater rotational drag and steric hindrance, resulting in slower relaxation dynamics and a broader orientational dispersion. A similar interpretation has been proposed to explain size-dependent magnetic responsiveness of GO photonic crystals.[6] It is also possible that larger nanosheets form a structural state analogous to the special columnar nematic arrangement.[15] In addition, other structural factors, including nanosheet undulations that induce local variations in intersheet spacing, may also contribute to the observed broadening.[18]

On the other hand, for nanosheets with the same lateral size, a decrease in the volume fraction leads to a shift of λ_{peak} toward longer wavelengths and increase in the lamellar spacing. The enlarged intersheet separation suggests that fewer lamellar periods can be accommodated within a cell of fixed thickness. Moreover, at low volume fractions, the distribution of lamellar spacing d across different domains may become broader, which in turn leads to a correspondingly wider reflection peak.

In summary, we systematically tuned the mean size of $Ti_{0.87}O_2$ nanosheets *via* sonication and analyzed the resulting structural color response using reflectance spectroscopy. Compared with large-sized nanosheets, deionized suspensions of small-sized nanosheets exhibited a dominant blue color and a narrower reflection bandwidth. This difference can be attributed to a more well-aligned lamellar texture formed under weak shear for smaller sheets, resulting in a narrower azimuthal distribution of the director and improved in-plane registry. In contrast, larger sheets, constrained by neighboring ones, are more difficult to rotate and align uniformly. The current study demonstrates that modulating the lateral size of 2D nanosheets is an effective strategy for enhancing the color purity of structural coloration.

Takayuki Kikuchi: methodology, validation, investigation, writing – original draft, visualization. Yasuo Ebina: investigation. Nobuyuki Sakai: writing – review & editing. Yoshiyuki Sugahara: writing – review & editing. Takayoshi Sasaki conceptualization, supervision, writing – review & editing. Renzhi Ma conceptualization, supervision, writing – review & editing.

This work was supported in part by the World Premier International Research Center Initiative (WPI), Ministry of Education, Culture, Sports, Science and Technology (MEXT), and CREST of the Japan Science and Technology Agency (JST) (Grant No. JPMJCR17N1 & JPMJCR22B1), Japan. R. M. acknowledges support from JSPS KAKENNHI (22H01916).

Conflicts of interest

There are no conflicts to declare.

Data availability

The data supporting this article have been included as part of the supplementary information (SI). Supplementary information is available. See DOI: https://doi.org/10.1039/d5cc06149k.

References

1 L. Onsager, *Ann. N. Y. Acad. Sci.*, 1949, **51**, 627–659.
2 (*a*) K. Sano, Y. S. Kim, Y. Ishida, Y. Ebina, T. Sasaki, T. Hikima and T. Aida, *Nat. Commun.*, 2016, **7**, 12559; (*b*) T. Kikuchi, Y. Ebina, N. Sakai, Y. Sugahara, T. Sasaki and R. Ma, *JACS Au*, 2025, **5**, 5207–5216.
3 (*a*) P. Ganter, K. Szendrei and B. V. Lotsch, *Adv. Mater.*, 2016, **28**, 7436–7442; (*b*) T. Gong, X. Zhang, Y. Fu, G. Zhou, H. Chi and T. Li, *Sens. Actuators, B*, 2018, **261**, 83–90.
4 (*a*) W. Hong, Z. Yuan and X. Chen, *Small*, 2020, **16**, 1907626; (*b*) N. Li, H. Zhang, Z. Chen and J. Wei, *J. Mater. Sci.*, 2022, **57**, 14310–14323.
5 (*a*) P. Li, M. Wong, X. Zhang, H. Yao, R. Ishige, A. Takahara, M. Miyamoto, R. Nishimura and H.-J. Sue, *ACS Photonics*, 2014, **1**, 79–86; (*b*) N. Miyamoto and S. Yamamoto, *ACS Omega*, 2022, **7**, 6070–6074.
6 D. Ogawa, Y. Nishina and K. Sano, *ChemPlusChem*, 2024, **89**, e202400449.
7 N. Miyamoto and T. Nakato, *J. Phys. Chem. B*, 2004, **108**, 6152–6159.
8 S. Saxena, T. A. Tyson, S. Shukla, E. Negusse, H. Chen and J. Bai, *Appl. Phys. Lett.*, 2011, **99**, 013104.
9 H.-J. Kim, M. Osada, Y. Ebina, W. Sugimoto, K. Tsukagoshi and T. Sasaki, *Sci. Rep.*, 2016, **6**, 19402.
10 T. Shibata, N. Sakai, K. Fukuda, Y. Ebina and T. Sasaki, *Phys. Chem. Chem. Phys.*, 2007, **9**, 2413–2420.
11 (*a*) M. Osada, T. Sasaki, K. Ono, Y. Kotani, S. Ueda and K. Kobayashi, *ACS Nano*, 2011, **5**, 6871–6879; (*b*) M. Osada, M. Itose, Y. Ebina, K. Ono, S. Ueda, K. Kobayashi and T. Sasaki, *Appl. Phys. Lett.*, 2008, **92**, 253110.
12 T. Maluangnont, K. Matsuba, F. Geng, R. Ma, Y. Yamauchi and T. Sasaki, *Chem. Mater.*, 2013, **25**, 3137–3146.
13 (*a*) H. N. W. Lekkerkerker and R. Tuinier, *Colloids and the Depletion Interaction*, Springer Nature, 2011; (*b*) E. Paineau, K. Antonova, C. Baravian, I. Bihannic, P. Davidson, I. Dozov, M. Impéror-Clerc, P. Levitz, A. Madsen, F. Meneau and L. J. Michot, *J. Phys. Chem. B*, 2009, **113**, 15858–15869.
14 (*a*) J. Park, J. Moon, H. Shin, D. Wang and M. Park, *J. Colloid Interface Sci.*, 2006, **298**, 713–719; (*b*) C. H. Lee, J. Yu, Y. Wang, A. Y. L. Tang, C. W. Kan and J. H. Xin, *RSC Adv.*, 2018, **8**, 16593–16602.
15 D. Yamaguchi, N. Miyamoto, T. Fujita, T. Nakato, S. Koizumi, N. Ohta, N. Yagi and T. Hashimoto, *Phys. Rev. E*, 2012, **85**, 011403.
16 Z. Xu and C. Gao, *ACS Nano*, 2011, **5**, 2908–2915.
17 (*a*) Y. Liu and P. Wu, *Adv. Sci.*, 2020, **7**, 2001269; (*b*) C. F. Dai, Q. L. Zhu, O. Khoruzhenko, M. Thelen, H. Bai, J. Breu, M. Du, Q. Zheng and Z. L. Wu, *Adv. Sci.*, 2024, **11**, 2402824.
18 T. Nakato, Y. Higashi, W. Ishitobi, T. Nagashita, M. Tominaga, Y. Suzuki, T. Iwai and J. Kawamata, *Langmuir*, 2019, **35**, 5568–5573.

